ChemComm
Chemical Communications

Accepted Manuscript

This article can be cited before page numbers have been issued, to do this please use: D. Blasi, V. Nicolai, R. M. Gomila, P. Mercandelli, A. Frontera and L. Carlucci, *Chem. Commun.*, 2022, DOI: 10.1039/D2CC03457C.

ROYAL SOCIETY OF CHEMISTRY

rsc.li/chemcomm

View Article Online
DOI: 10.1039/D2CC03457C

COMMUNICATION

Unprecedented {d_{z^2}-$Cu^{II}O_4$}···π-hole interactions: the case of a cocrystal of Cu(II) bis-β-diketonate complex with 1,4-diiodotetrafluoro-benzene

Received 00th January 20xx,
Accepted 00th January 20xx

DOI: 10.1039/x0xx00000x

Delia Blasi,[a] Valentina Nicolai,[a] Rosa M. Gomila,[b] Pierluigi Mercandelli,[a] Antonio Frontera*[b] and Lucia Carlucci*[a]

Cocrystallization of bis-[1-(4-pyridyl)butane-1,3-dionato]copper(II) (1) complex and 1,4-diiodoperfluorobenzene in the presence of pyridine yields to a 1:1 cocrystal where both the σ and π-holes of 1,4-diiodoperfluorobenzene play a role. The crystal structure shows short arene CuO_4···π-hole stacking contacts, where the {d_{z^2}-$Cu^{II}O_4$} moiety functions as an integrated five-center π-hole acceptor. DFT calculations combined with quantum theory of atoms-in-molecules and noncovalent interaction plot analyses, corroborated the structure-defining role of the {d_{z^2}-$Cu^{II}O_4$}···π-hole contacts.

Recent investigations have demonstrated that square-planar d^8–metal complexes are convenient binding sites for establishing diverse noncovalent interactions.[1] Despite their formal positive charge, metal centres (mostly late transition metals) can function as d_{z^2}-nucleophiles toward σ- and π-hole donors.[2] The nucleophilicity of metal complexes has been already disclosed for Rh^{I}, Ni^{II}, Pd^{II}, and Pt^{II} in σ-hole hydrogen, halogen and chalcogen bonding.[3–7] For π-hole bonding, several investigations have also demonstrated that "pure" d_{z^2}-M···π-hole interactions (no other interaction involved) have a strong structure directing role in the solid state of Pd^{II} and Pt^{II} complexes. This is due to the strong d_{z^2}-donating ability of Pd^{II} and Pt^{II} metal centers.[8,9] More recently, the formation of d^8[M]···π-hole interactions for the rather weak nucleophilic Ni^{II} centers has been also demonstrated, where the d_{z^2}-nucleophilicity is enhanced by the presence of strong electron-donor ligands (dithiocarbamates).[10] Apart from d^8[M]···σ,π-hole interactions, few investigations have demonstrated the relevance of σ-hole···d^{10}[Au^{I}] interactions in the solid state.[2] In the case of d^{10}-[M] (M = Cu^{I}, Ag^{I} and Au^{I}) linear complexes, both the d_{xy} and $d_{x^2-y^2}$ atomic orbitals are sterically accessible and available to function as electron donors.

Taking into account all these issues, we envisaged that square pyramidal complexes of d^9[Cu], which have not previously considered, could be logical candidates for a study of π-hole···d_{z^2}[Cu] interactions (see Scheme 1). The unpaired electron resides in the $d_{x^2-y^2}$ orbital (basal plane) and the high energy and doubly occupied d_{z^2}[Cu] atomic orbital should have enough nucleophilicity to establish d_{z^2}[Cu]···π-hole interactions. In addition, we also anticipated that the utilization of a good σ-hole acceptor like pyridine as pendant arm of the copper complex would facilitate the formation of supramolecular polymers.

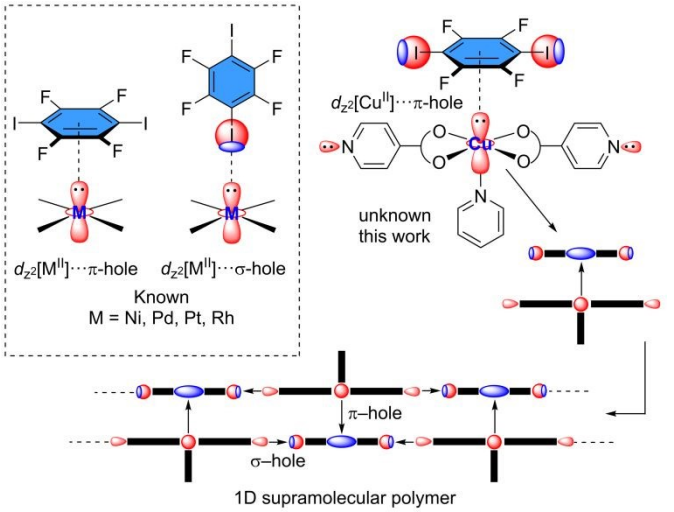

Scheme 1 Left: known d^8[M]···σ,π-hole. Right: unknown d^9[Cu]···π-hole interactions reported herein. Bottom: crystal engineered supramolecular polymer based on classical halogen bonds and unconventional d^9[Cu]···π-hole interactions

Herein we report the synthesis and X-ray characterization of a co-crystal formed by copper(II) bis[4-oxo-4-(pyridin-4-yl)but-2-en-2-olate] complex **1** and 1,4-diiodoperfluorobenzene (FIB), see Fig. 1. The latter was chosen as a ditopic π-/σ-hole donor and the former as a ditopic lone pair donor via de pyridine arms and as mono-facial {CuO_4} electron donor. The utilization of the {d_{z^2}-CuO_4} core as electron donor is, as far as our knowledge

[a] Dipartimento di Chimica, Università degli Studi di Milano, via C. Golgi 19, 20133 Milano, Italy. E-mail: lucia.carlucci@unimi.it
[b] Departament de Química, Universitat de les Illes Balears, Crta de Valldemoss km 7.5, 07122 Palma de Mallorca, Baleares, Spain. E-mail: toni.frontera@uib.es
Electronic Supplementary Information (ESI) available: Synthesis, IR spectrum, X-ray details and theoretical methods. See DOI: 10.1039/x0xx00000x

extends, unprecedented in the literature. In fact, the Cambridge structural database (CSD), which is a large depot of geometrical information, was inspected suggesting that there is not any square pyramidal structure of Cu(II) in the database where the metal center interacts with a partially fluorinated and electron deficient aromatic ring (at least four F-atoms).

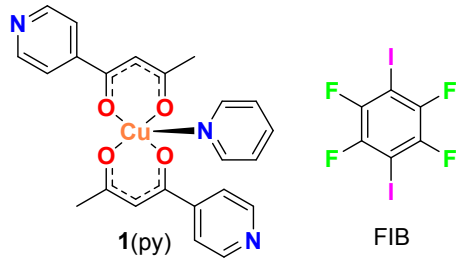

Fig. 1 Co-formers used in this work

The CSD was further inspected, expanding the search to more common square planar Cu(II) complexes. As a result, only one structure was found where the Cu(II) atom is close to a fluorinated ring, which is represented in Fig. 2. It corresponds to refcode ERARUN,[11] where the Cu(II) ion is coordinated to the octafluoro-dibenzotetra-aza[14]annulene ligand. This perfectly planar complex propagates in the solid state forming infinite 1D stacked columns where Cu ion is located between two tetrafluorophenyl rings equidistant at 3.359 Å from the ring centres.

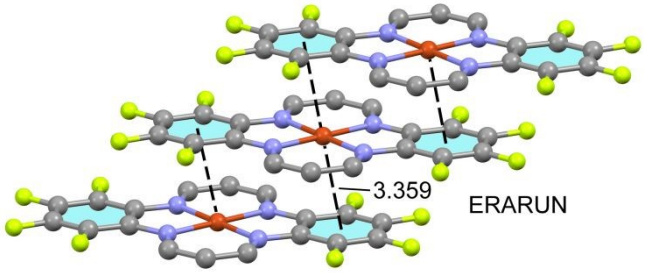

Fig. 2 Partial view of the X-ray structure with CSD refcode **ERARUN**. Cu···ring centroid distance is given in Å.

Emerald block single crystals suitable for XRD analysis of herein reported cocrystal **1**(py)·(FIB) were obtained by slow evaporation of an acetone solution containing the Cu(II) bis-diketonate complex and FIB in 1:1 molar ratio and a large excess of pyridine (see ESI for X-ray diffraction experimental details). To obtain cocrystal **1**(py)·(FIB) the large excess of pyridine was necessary and attempt to cocrystallize the copper complex with FIB in the absence of pyridine failed. This is due to the strong tendency of the pyridyl groups of chelated diketonate ligands to give intermolecular coordination on the axial positions of copper atoms producing polymeric structures well documented in the literature.[12]

Two views (perspective and overhead) of the asymmetric unit of the cocrystal are given in Fig. 3. The most interesting feature is the occurrence of the {$d_{z}2$-CuO_4}···arene short contact (distances to the mean plane of FIB are: Cu···arene: 3.5313(11) Å, O···arene: 3.138–3.418 Å). These distances are similar to those recently reported for cocrystals of group 10 metal dithiocarbamates with electron deficient arenes.[10] The overhead view (Fig. 3b) shows that the {$d_{z}2$-CuO_4}···π-hole interaction slightly deviates from the π-hole centroid to give CuO_4···arene contacts opposite to the Cu–Py bond (Fig. 3b). This type of M···arene structure-directing interactions have been described for square planar complexes (for group 10) but they have not described before neither for square-planar nor square-pyramidal Cu-complexes.

Another interesting feature of the {$d_{z}2$-CuO_4}···π-hole assembly shown in Fig. 3b is that the directionality of the C–I bonds of FIB and the pyridinyl lone pairs is almost perfectly parallel (see small arrows in Fig. 3b) thus adequate for the propagation of the 1:1 π-hole adducts generating 1D supramolecular assemblies assisted by C–I···N_{py} halogen bonds. The 1D supramolecular polymer is represented in Fig. 4, where two slightly different halogen bonds are formed. That is, the I···N distances are 2.793(2) and 2.845(2) Å, which are shorter than the sum of van der Waals radii.[13] Moreover, both ∠C–I···N angles are greater than 178°, thus exhibiting strong directionality, as expected for halogen bonds.[14] Both σ- and π-hole interactions clearly govern the solid state architecture of the cocrystal.

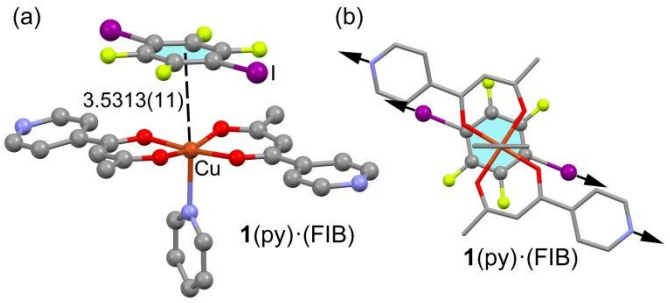

Fig. 3 Perspective (a) and overhead (b) views of the **1**(py)·(FIB) cocrystal. The distance is measured from the Cu-atom to the ring centre.

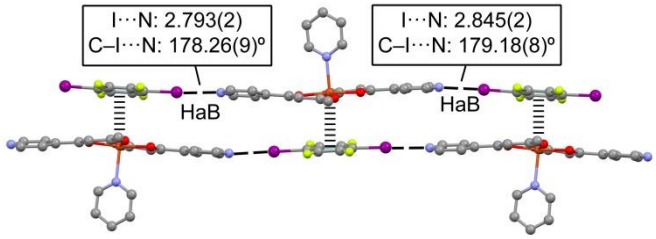

Fig. 4 1D supramolecular polymer observed in the solid state of the **1**(py)·(FIB) cocrystal. Distances in Å.

To verify the nucleophilic/electrophilic properties of **1**(py) and FIB, computation of the molecular electrostatic potential (MEP) was performed. The MEP surfaces are gathered in Fig. 5 disclosing that in **1**(py) the MEP minimum is located at the N-atoms of the pyridine rings (–36.4 kcal/mol). The MEP is also large and negative between the O-atoms coordinated to Cu(II) metal centre. Remarkably, the MEP is also negative over the entire {$d_{z}2$-CuO_4} unit, ranging from –8.8 kcal/mol over the Cu-atom to –18.1 kcal/mol over the O-atoms, thus confirming the

nucleophilic character of the d_{z^2} orbital, which is likely enhanced by the presence of the Cu–N coordination bond at the opposite side, as further discussed below. In FIB, the MEP maximum is located at the σ-holes of the iodine atoms (+31.4 kcal/mol). The MEP value at the π-hole is significantly smaller (+13.8 kcal/mol, see Fig. 5b). This MEP analysis reveals that the C–I···N halogen bonding interactions are the most favoured from an electrostatic point of view. This MEP surface analysis also demonstrates that the {d_{z^2}-CuO_4}···π-hole described above is also electrostatically favoured.

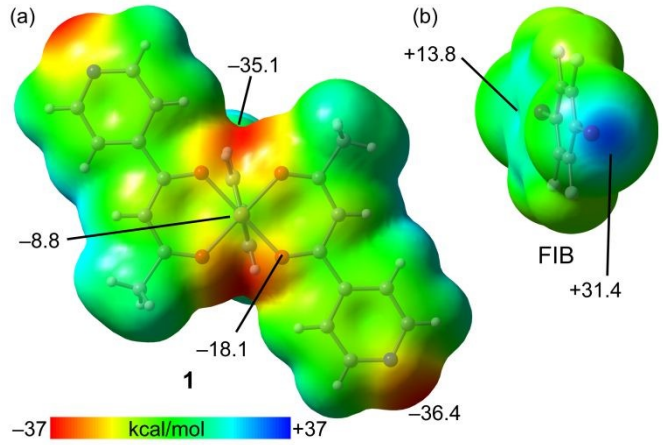

Fig. 5 MEP surfaces of **1**(py) (a) and FIB (b) using the same scale (±37 kcal/mol) at the RI-BP86-D3/def2-TZVP level of theory. The values at selected points of the surfaces are given in kcal/mol. Isovalue 0.001 a.u.

In order to further inspect the energetic features of the supramolecular assemblies shown in Fig. 4 and the ability of the d^9-Cu(II) metal participate in d_{z^2}-Cu···π-hole interactions, DFT calculations were carried out (see ESI for computational details). In addition to the energetic evaluation of the assemblies, a combination QTAIM[15] and NCIplot[16] analyses were used since both computational tools are adequate for the representation of noncovalent interactions in real space.

The π-hole 1:1 adduct is represented in Fig. 6a, where the intermolecular distribution of bond critical points (CPs, indicated as red spheres) and bond paths is shown. The superimposed NCIplot reduced density gradient (RDG) isosurface is also represented. It can be observed that the NCIplot RDG isosurface is very extended, embracing the whole region between the FIB molecule and complex **1**. This large complementarity of both molecules where one entire face of FIB is in contact with **1** explains the strong interaction energy (ΔE_1 = –17.3 kcal/mol). In fact, there are eleven bond CPs interconnecting both compounds, including the CuO_4 core. The density values at the bond CPs connecting the CuO_4 core to FIB are indicated in Fig. 6a, showing quite similar values, varying from 4.11 x 10^{-3} to 4.70 x 10^{-3} a.u. for the three CPs connecting the O-atoms to the C-atoms and 4.71 x 10^{-3} a.u. for the CP connecting the Cu to the C-atom. Such similar ρ values suggest that the contribution of the Cu···C and O···C contacts to the interaction energy is similar. For the rest of CPs the values are given in Table S2 (ESI) along with further discussion regarding the bond paths interconnecting the O and I-atoms.

It is worthy to highlight that the spin density plot of the adduct (see Fig. 6b) shows that the unpaired electron is mainly located at the $d_{x^2-y^2}$ Cu-orbital, as expected for square pyramidal complexes, with some spin delocalization to the O-atoms of the ligand directly bonded to copper. There is not any spin delocalization in the FIB molecule, thus suggesting that this orbital does not participate in the binding mechanism and that the computed interaction energy of the adduct is not influenced by spin density transfer effects. Further analysis of molecular orbitals of compound **1**(Py) is given in the ESI (Fig. S2) showing the polarization of the d_{z^2} orbital opposite to the C–N(py) bond, and supporting the enhanced nucleophilicity of this orbital due to the presence of the axial pyridine ligand.

The halogen bonding N···I σ-hole interactions have been also analysed theoretically (see Fig. 6e). The interaction energy of the **1**(py)·$(FIB)_2$ HaB trimer is ΔE_2 = –16.6 kcal/mol, disclosing the strong nature of the HaBs (≈–8.3 kcal/mol) in line with the MEP surface analysis and the dark blue colour of the NCIplot isosurfaces (signλ_2 x ρ = –0.35 a.u.) that are located coincident with the bond CPs connecting the I and N-atoms. The π-hole 1:1 adduct is stronger than the σ-hole likely due to the larger contact surface between both counterparts.

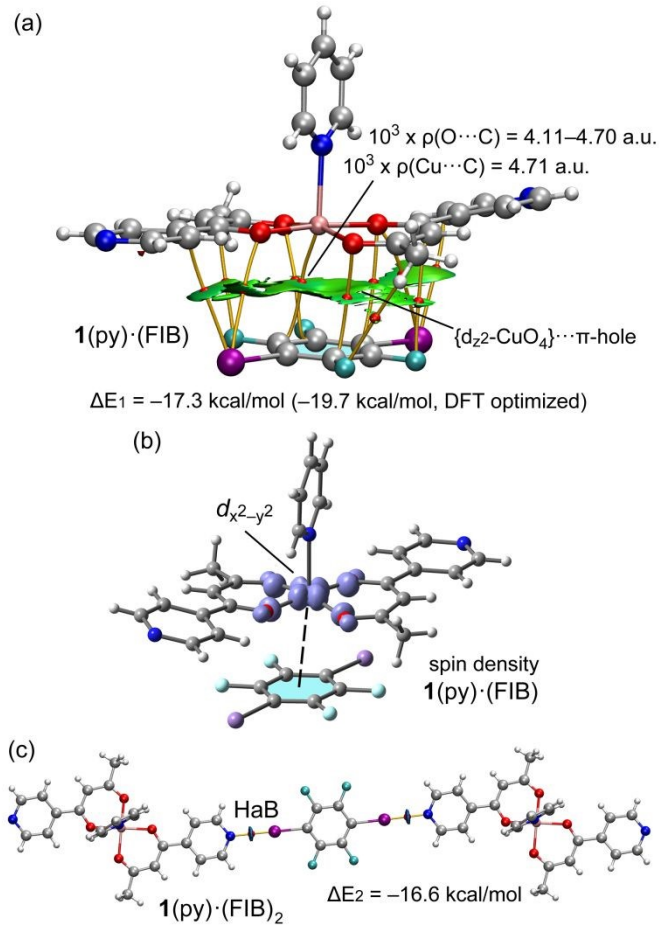

Fig. 6 (a) Visualization of QTAIM bond CPs (in red), bond paths (orange lines) and NCI analyses of the π-hole 1:1 adduct. For NCIPlot, interactions, RDG surfaces with 0.5 a.u. values were coloured from blue [sign(λ_2)ρ(r) = –0.03 e $Bohr^{-3}$] to red [sign(λ_2)ρ(r) = +0.03 e $Bohr^{-3}$]. (b) Spin density plot (isovalue 0.004 a.u.) of the **1**(py)·(FIB) adduct. (c) Visualization of QTAIM bond CPs (in red), bond paths (orange lines) and NCI analyses of the σ-hole 1:2 adduct. The NCIPlot settings described in section (a) were used.

In order to further demonstrate that the formation of the {$d_{z}2$-CuO_4}···π-hole interaction is not simply a consequence of packing effects, we have fully optimized the π-hole 1:1 adduct using DFT calculations (RI-BP86-D3/def2-TZVP level of theory). Gratifyingly, the X-ray and DFT geometries of the dimer are very similar (see Fig. S3), regarding the relative orientation of both monomers and the complementarity. Remarkably, {$d_{z}2$-CuO_4}···π-hole interaction is even reinforced in the gas phase. That is, the main difference between X-ray and *in silico* geometries is that the Cu···arene and O···arene shortens in the DFT optimized adduct around 0.2 Å compared to the X-ray one, in line with the strongest binding energy found for the theoretical one (–19.7 kcal/mol). This shortening and reinforcement is likely due to the absence of additional interactions in the isolated dimer, opposite to the solid state environment. It is also worth mentioning that the experimental and theoretical Cu–O and Cu–N coordination bond distances in **1**·(Py) are almost identical (differences < 0.01 Å for Cu–O and < 0.04 Å for Cu–N bonds) thus validating the level of theory used in this work. Finally, it is interesting to highlight that the composition of the the $d_{z}2$ orbital orbital (see Fig. S2) does not change in the optimized structure. This orbital is the result of mixing with the $4p_z$ orbital and it is naturally polarized because it has Cu-N antibonding character, as in any square pyramidal complex.

In conclusion, a new co-crystal has been designed and synthesized to demonstrate the ability of the {$d_{z}2$-CuO_4} moiety to act as an integrated electron donor. It can be concluded that square-pyramidal d^9-copper centre with sterically unhindered chelating ligands (i.e., acetoacetonate derivatives) in the basal plane is a suitable $d_{z}2$-nucleophilic partner toward a prototypical π-hole donating aromatic (FIB). The oxygen atoms coordinated to Cu(II) impels the existence of additional contacts with the electron-deficient FIB, so the interaction can be better defined as {$d_{z}2$-CuO_4}···π-hole interaction. Energetically, it is competitive with the classical halogen bonds formed between the pyridine arms and the iodine atoms and, consequently, both the HaBs and π-holes interactions equally contribute to the formation of the 1D supramolecular polymer observed in the solid state of **1**(Py)·(FIB). Finally, it should be emphasized the $d_{z}2$-nucleophilicity of Cu(II) revealed in this study is enhanced by the polarization of this atomic orbital due to the presence of the axial ligand, as disclosed by the DFT calculations.

Acknowledgments: This research was funded by the Italian MUR (PRIN2020: 2020Y2CZJ2_004) and by MICIU/AEI of Spain (project PID2020-115637GB-I00 FEDER funds). We thank the "centre de tecnologies de la informació" (CTI) at the University of the Balearic Islands for computational facilities.

Conflicts of interest: There are no conflicts to declare

Author contributions: D.B, V.N. Synthesis, investigation; R.M.G.: DFT calculations; P.M., L.C. X-ray diffraction; A. F., L.C.: investigation, writing original draft, conceptualization, funding.

Notes and references

View Article Online
DOI: 10.1039/D2CC03457C

1 (a) I. Alkorta, J. Elguero and A. Frontera, *Crystals*, 2020, **10**, 180; (b) R. M. Gomila, A. Bauzá and A. Frontera, *Dalton Trans*., 2022, **51**, 5977-5982; (c) A. Frontera, A. Bauza, *Int. J. Mol. Sci*., 2022, **23**, 4188.

2 (a) D. M. Ivanov, N. A. Bokach, V. Y. Kukushkin and A. Frontera, *Chem. Eur. J*., 2021, **28**, e202103173; (b) I. Benito, R. M. Gomila and A. Frontera, *CrystEngComm*, 2022, **24**, 4440-4446.

3 U. Dabranskaya, D. M. Ivanov, A. S. Novikov, Y. V. Matveychuk, N. A. Bokach and V. Y. Kukushkin, *Cryst. Growth Des*., 2019, **19**, 1364–1376.

4 (a)A. A. Eliseeva, D. M. Ivanov, A. V. Rozhkov, I. V. Ananyev, A. Frontera and V. Y. Kukushkin, *JACS Au*, 2021, **1**, 354–361; (b) D. M. Ivanov, A. S. Novikov, I. V. Ananyev, Y. V. Kirina and V. Y. Kukushkin, *Chem. Commun*., 2016, **52**, 5565–5568; E. A. Katlenok, M. Haukka, O. V. Levin, A. Frontera and V. Y. Kukushkin, *Chem. – Eur. J*., 2020, **26**, 7692–7701.

5 E. A. Katlenok, A. V. Rozhkov, O. V. Levin, M. Haukka, M. L. Kuznetsov and V. Y. Kukushkin, *Cryst. Growth Des*., 2021, 21, 1159–1177; A. V. Rozhkov, D. M. Ivanov, A. S. Novikov, I. V. Ananyev, N. A. Bokach and V. Y. Kukushkin, *CrystEngComm*, 2020, **22**, 554–563; Z. M. Bikbaeva, D. M. Ivanov, A. S. Novikov, I. V. Ananyev, N. A. Bokach and V. Y. Kukushkin, *Inorg. Chem*., 2017, **56**, 13562–13578.

6 M. Baya, Ú. Belío and A. Martín, *Inorg. Chem*., 2014, **53**, 189–200; M. K. Yadav, G. Rajput, L. B. Prasad, M. G. B. Drew and N. Singh, *New J. Chem*., 2015, **39**, 5493–5499; F. Kraus, H. Schmidbaur and S. S. Al-juaid, *Inorg. Chem*., 2013, **52**, 9669–9674.

7 A. V. Rozhkov, E. A. Katlenok, M. V. Zhmykhova, A. Y. Ivanov, M. L. Kuznetsov, N. A. Bokach and V. Y. Kukushkin, *J. Am. Chem. Soc*., 2021, **143**, 15701–15710.

8 A. V. Rozhkov, I. V. Ananyev, R. M. Gomila, A. Frontera and V. Y. Kukushkin, *Inorg. Chem*., 2020, **59**, 9308–9314.

9 A. V. Rozhkov, M. A. Krykova, D. M. Ivanov, A. S. Novikov, A. A. Sinelshchikova, M. V. Volostnykh, M. A. Konovalov, M. S. Grigoriev, Y. G. Gorbunova and V. Y. Kukushkin, *Angew. Chem., Int. Ed*., 2019, **58**, 4164–4168.

10 L. E. Zelenkov, A. A. Eliseeva, S. V. Baykov, D. M. Ivanov, A. I. Sumina, R. M. Gomila, A. Frontera, V. Yu. Kukushkin and N. A. Bokach, *Inorg. Chem. Front*., 2022, **9**, 2869-2879.

11 L. Pilia, Y. Shuku, S. Dalgleish, K. Awaga, N. Robertson, *ACS Omega*, 2018, **3**, 10074.

12 (a) G.-G. Hou, Y. Liu, Q.-K. Liu, J.-P. Ma and Y.-B. Dong Chem. Commun., 2011, 47, 10731–10733; (b) K. V. Domasevitch, V. D. Vreshch, A. B. Lysenko and H. Krautscheid, *Acta Cryst*., 2006, C62, m443–m447; (c) C. J. McMonagle, P. Comar, G. S. Nichol, D. R. Allan, J. González, J. A. Barreda-Argüeso, F. Rodríguez, R. Valiente, G. F. Turner, E. K. Brechin and S. A. Moggach, *Chem. Sci*., 2020, **11**, 8793–8799

13 A. Bondi, *J. Phys. Chem*., 1964, **68**, 441–451.

14 (a) G. Cavallo, P. Metrangolo, R. Milani, T. Pilati, A. Priimagi, G. Resnati, G. Terraneo, *Chem. Rev*., 2016, **116**, 2478–2601; (b) A. Bauzá, D. Quiñonero, A. Frontera and P. M. Deyà, *Chem. Phys. Phys. Chem*., 2011, **13**, 20371-20379

15 R. F. W. Bader, *Chem. Rev*., 1991, **91**, 893–928.

16 J. Contreras-García, E. R. Johnson, S. Keinan, R. Chaudret, J.-P. Piquemal, D. N. Beratan and W. Yang, *J. Chem. Theor. Comput*., 2011, **7**, 625–632.